Energy Reports 9 (2023) 159–164

Contents lists available at ScienceDirect

Energy Reports

journal homepage: www.elsevier.com/locate/egyr

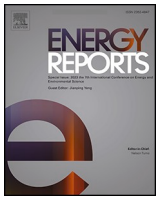

2023 8th International Conference on Sustainable and Renewable Energy Engineering (ICSREE 2023) 11–13 May, Nice, France

Efficiency-enhanced DC-excited Vernier reluctance machine with reduced excitation coils for electric vehicles

Ziqi Huang [a], Xing Zhao [b], Shuangxia Niu [a,*], Yuanxi Chen [a], Xingwei Zhou [c], Chao Gong [a]

[a] The Hong Kong Polytechnic University, Kowloon, Hong Kong
[b] Department of Electronic Engineering, University of York, UK
[c] Department of Electrical Engineering, Hohai University, Nanjing, China

ARTICLE INFO

Keywords:
DC copper loss
Efficiency
DC-excited Vernier reluctance machine

ABSTRACT

Due to its good mechanical robustness and field control capacity, the DC-excited Vernier reluctance machine (DC-VRM) is a promising candidate for electrical vehicle propulsion. However, the conventional design of this machine suffers from large excitation copper loss and leading to low efficiency, due to an identical distribution of DC excitation coils at the stator side. This paper proposes a novel efficiency-enhanced DC-VRM. The key technology is based on the flux modulation mechanism to reduce DC field coils and mitigate DC copper loss while keeping the excitation ability and power density not sacrificed. In this paper, the machine configuration and operation principle are introduced. A combination of the magneto-static finite element and the analytical method is used to quantitatively analyze the contribution of different harmonics on the phase EMF under two different DC layouts. The feasibility of the proposed topology is further verified by a transient finite element analysis, which proves that, with the same design parameters, the proposed design achieves higher back EMF and output torque per DC copper loss. Therefore, this new topology enhances efficiency and can be a more promising non-PM machine for EVs.

1. Introduction

Due to a limited supply of the rare-earth permanent magnet (PM) and its increasing cost burden, developing reduced or non-PM machines with high performance for electric vehicles (EV) is an important research topic [1]. Switching reluctance machine (SRM) [2–4] is a potential solution. However, it has a relatively large torque ripple due to its half-cycle-conducting characteristic [5]. Doubly-fed doubly salient machine (DFDSM), which owns a similar structure to SRM but employs extra DC excitation at the stator side, has also been studied [6]. However, its torque ripple is still unacceptable caused of a bipolar flux characteristic [7]. To address the issue in DFDSM, a new topology, Variable flux reluctance machine (VFRM) is proposed [8,9]. VFRM provides an alternating excitation flux, similar to conventional AC synchronous machines. Therefore, it achieves a smoother torque when driven by the sinusoidal current. Recently, it has been revealed that the operation principle of VFRM can be interpreted based on the flux modulation theory [10]. Meanwhile, more possible slot pole combinations are discovered with such a new perspective, including some new cases with distributed armature winding. They are clarified as the DC-excited Vernier reluctance machine (DC-VRM).

Vary from some researches on torque density [11], torque ripple [12], and power factor [13] of DC-VRM. This paper focuses on a distinct issue in DC-VRM: its energy consumption in the DC field terminal, which leads to a nonnegligible copper loss and thus reduced efficiency. Hence, how to reduce excitation copper loss and increase efficiency in DC-VRM, is a meaningful exploration to broaden its potential for EVs, in which the efficiency of the propulsion machine is one of the leading factors to determine the practical driving range.

Based on the flux modulation principle, this paper proposes a new efficiency-enhanced DC-VRM for EV propulsion. This paper is organized as follows. In Section 2, the machine configuration and its operation principle are first introduced. Then in Section 3, based on a magneto-static finite element and analytical combined method, the influence of different DC layouts is quantitatively assessed by separating the contribution of different harmonics on phase EMF. Further, in Section 4, the feasibility of the proposed design is verified by a transient finite element analysis. Some conclusions are drawn in Section 5.

* Corresponding author.
E-mail address: shuangxia.niu@polyu.edu.hk (S. Niu).

https://doi.org/10.1016/j.egyr.2023.09.111
Received 30 August 2023; Accepted 19 September 2023
Available online 29 September 2023

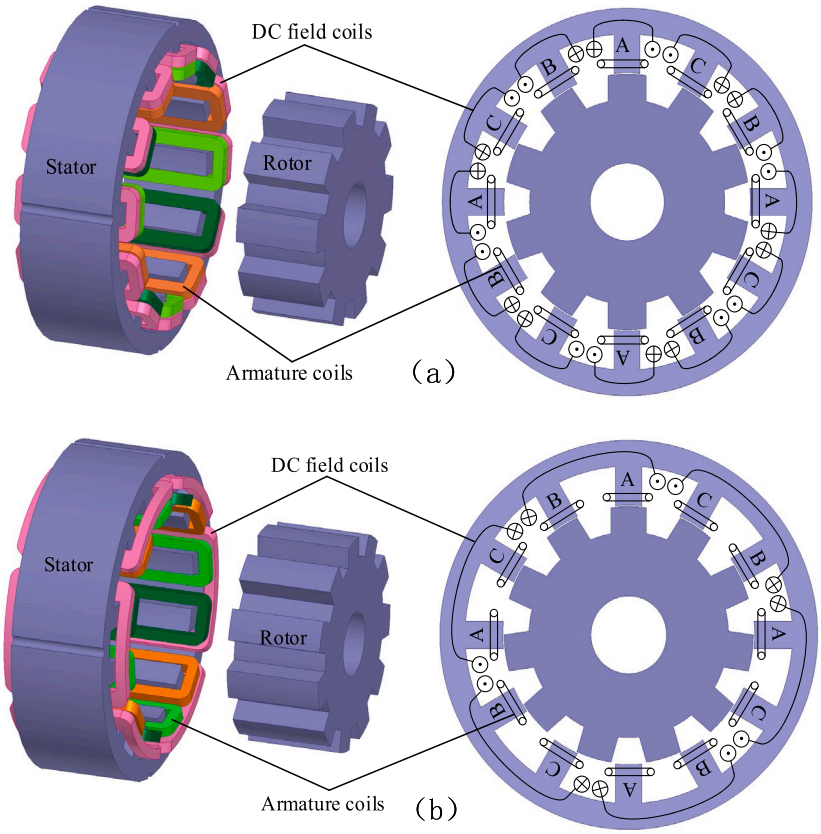

Fig. 1. DC-excited Vernier reluctance machine. (a) Existing. (b) Proposed.

2. Machine configuration and operation principle

The existing design and proposed new design for DC-VRM are presented in Fig. 1(a) and (b), respectively. They both generally employ two sets of windings at the stator side: DC field and AC armature. The rotor consists of only iron cores without any excitation components arranged. Therefore, DC-VRM owns excellent mechanical robustness, good field control ability by DC terminal and thus a wide speed range, which makes it a potential solution for EV propulsion.

It is further noticed, the critical difference between the two topologies is the layout of DC coils. In the existing topology, every DC coil is identically wounded on each stator tooth, while it is wounded on two stator teeth in the proposed design. Obviously, the total number of DC coils is halved. Besides, caused by the change of DC layout, the slot pole combination and winding configuration in the proposed topology also become different.

In general, the operation principle for two topologies can be illustrated by the flux modulation mechanism. Specifically, due to the rotor saliency effect, the magnetic field generated by the DC field source is not uniform. Instead, a number of harmonics will be produced in the air gap and their pole pair number (PPN) [14] can be predicted by

$$PPN_{mk} = |mp_s + kp_r| \\ m = 1, 3, 5\ldots, k = 0, \pm1, \pm2, \pm3\ldots \tag{1}$$

where p_s is the PPN of the DC field source, p_r is the number of rotor salient poles. Further, the corresponding rotational velocity of each harmonic component is

$$\omega_{m,k} = \frac{kp_r}{mp_s + kp_r}\omega_r \tag{2}$$

where ω_r is the rotor rotational velocity.

With this flux modulation effect [15], DC-excited harmonics with the same PPN and the same rotational velocity with those produced by the armature field will interact with each other. To transmit the highest electromagnetic torque, the PPN of the DC field source, the rotor pole number as well as the PPN of armature winding p_a, are governed by

$$p_r = p_s + p_a \tag{3}$$

Using a 12-slot stator as a design element, the PPN of the DC field source in the existing topology is 6, while that in the proposed topology is 3. The selection of rotor pole numbers in DC-VRM is relatively flexible. In this paper, the rotor pole number in the existing topology is selected as 10. Accordingly, based on (3), the PPN of armature winding can be derived as 4. This is a typical design for DC-VRM and has been widely investigated in kinds of literature. For the proposed topology, the rotor pole number is artificially selected as 11 in this paper and thus the PPN of armature winding is 8. In this case, the armature winding of two topologies is actually the same, accordingly, the copper loss of armature winding in two topologies can be easily kept the same at the design stage. Therefore, the influence of DC copper loss and machine efficiency can be more clearly evaluated for these two counterparts as given in Fig. 1, in which the main difference between them is the DC layout, from a structural perspective.

3. Contribution evaluation of different harmonics with two different DC layouts

With DC coils halved in the proposed design, the copper loss of DC field winding can be obviously reduced when applied by the same current excitation. However, its influence on the back EMF and torque density should be clearly studied. In this part, the combination of the magneto-static finite element and the analytical method is used for a fast and quantitative evaluation of the contribution of different DC field harmonics in two different topologies.

Firstly, the air gap magnetic field produced by two different DC

layouts can be quickly calculated by a magnetostatic finite element method, as plotted in Fig. 2. To more clearly show the influence of different DC layouts, the rotor modulation effect is not considered, and all the dimension parameters are maintained.

Two different DC layouts methods base on the same topology. It can be seen, with the DC coils reduced by half, a uniform excitation magnetic field can be still established along the air gap circumference, which means, the proposed topology with halved DC coils, is also able to realize an effective flux modulation operation if the rotor salient poles and armature winding are reasonably designed. Further, the air gap flux density of two DC layouts as well as its FFT analysis, are presented in Fig. 3. It can be found, regardless of DC layout, the dominant harmonics excited by the DC field source are always the fundamental, third-order and fifth-order DC field harmonics. Further, with DC coils halved, the spectrum of DC field harmonics also changes. Specifically, the PPN of fundamental, third-order and fifth-order DC field harmonics are all halved. Besides, the amplitude of the fundamental DC field harmonic is reduced, while that of the third and fifth-order components increases.

Without the modulation of rotor salient poles, the magnetic field excited by the DC field source is always stationary. However, after the rotor modulation effect, both stationary and rotational harmonic components would be produced in the air gap. Fig. 4 presents the DC magnetic field after rotor modulation. It can be found that the magnetic field distribution is no longer uniform along the air gap circumference, caused by the rotor modulation effect. Further, the air gap flux density is also calculated and presented in Fig. 5, along with the corresponding FFT analysis. Compared with Fig. 3, a lot of new harmonics are produced. As denoted in Fig. 5, the sub-harmonics excited by the fundamental DC field harmonics are classified into Group I, while those generated by the third-order and fifth-order DC field harmonics are classified into Group II and Group III, respectively.

To investigate the contribution of each harmonic component on the back EMF of one phase winding. The winding factor of each harmonic component [16] should be calculated by

$$\begin{cases} k_{pn} = cos(n\varepsilon/2) \\ k_{dn} = \dfrac{sin(mn\gamma/2)}{msin(n\gamma/2)} \\ k_{wn} = k_{pn}k_{dn} \end{cases} \tag{4}$$

where ε is the angle by which coils are short-pitched. γ is the slot angle. m is the coil number in one phase spread. n is the order of harmonics. k_{pn} is the pitch factor for the nth harmonic. k_{dn} is the distribution factor for the nth harmonic. k_{wn} is the final winding factor. For 12-slot 8-pole armature winding employed in this paper, $\varepsilon = 60°$, $\gamma = 120°$, $m = 1$. Further, the induced phase EMF by the nth harmonic component can be expressed as

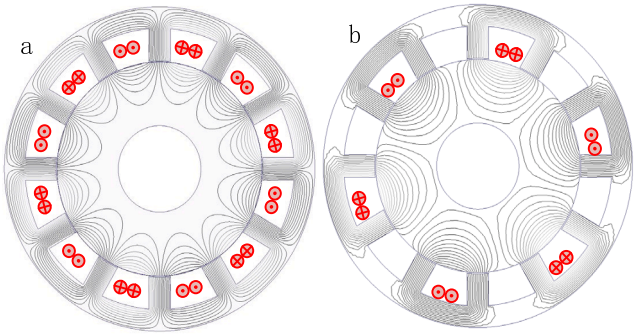

Fig. 2. No load magnetic field produced by two different DC layouts, before rotor modulation. (a) Existing. (b) Proposed.

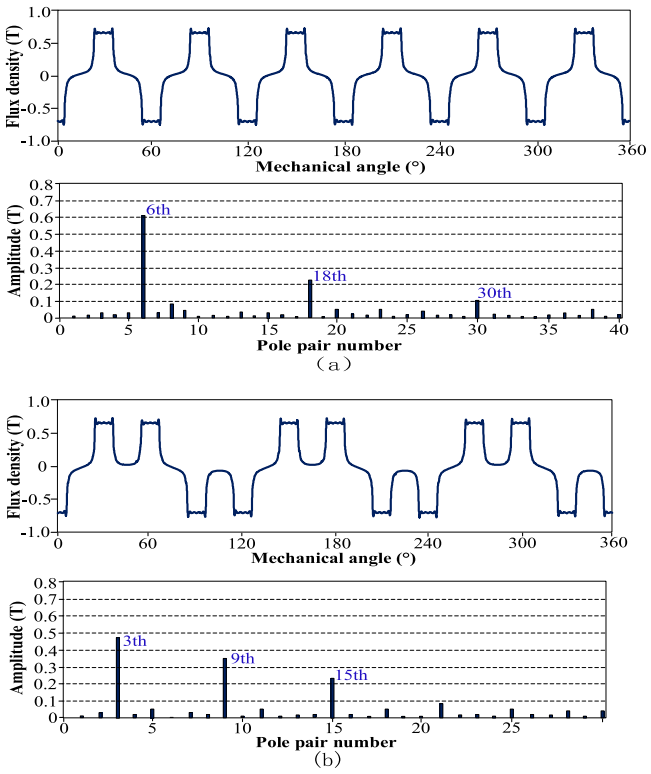

Fig. 3. Air gap flux density and FFT analysis of the magnetic field produced by two different DC layouts, before rotor modulation. (a) Existing. (b) Proposed.

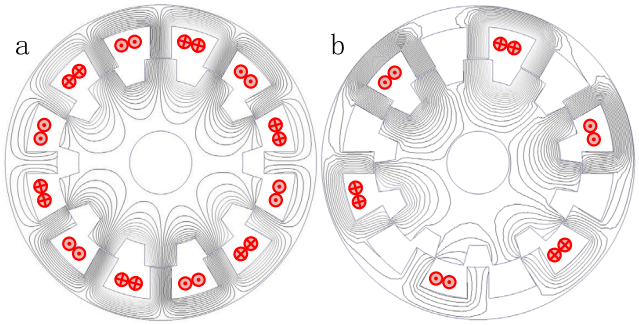

Fig. 4. No load magnetic field produced by two different DC layouts, after rotor modulation. (a) Existing. (b) Proposed.

$$E_{phn} = \frac{4.44k_{wn}T_{ph}B_{mn}DLN}{60} \tag{5}$$

where T_{ph} is the total turn number of one phase winding, B_{mn} is the amplitude of air gap flux density for nth harmonics. D is the diameter of the air gap circumference. L the stack length. N is the rotor rotational speed. The final synthetic phase EMF can be deduced as

$$E_{ph} = \sqrt{\left(E_{ph1}^2 + E_{ph2}^2 + E_{ph3}^2 + \cdots\cdots\right)} \tag{6}$$

Based on the above method, the contribution of each harmonic component on the phase EMF is calculated for two topologies and presented in Tables 1 and 2, respectively. It can be seen, in the proposed design with DC coils halved, the contribution of the fundamental DC field harmonic on EMF is reduced from 83.7% to 70.6%, while that of the third-order DC field harmonic is increased from 13.1% to 19.9%, and that of the fifth-order DC field harmonic is increased from 2.4% and

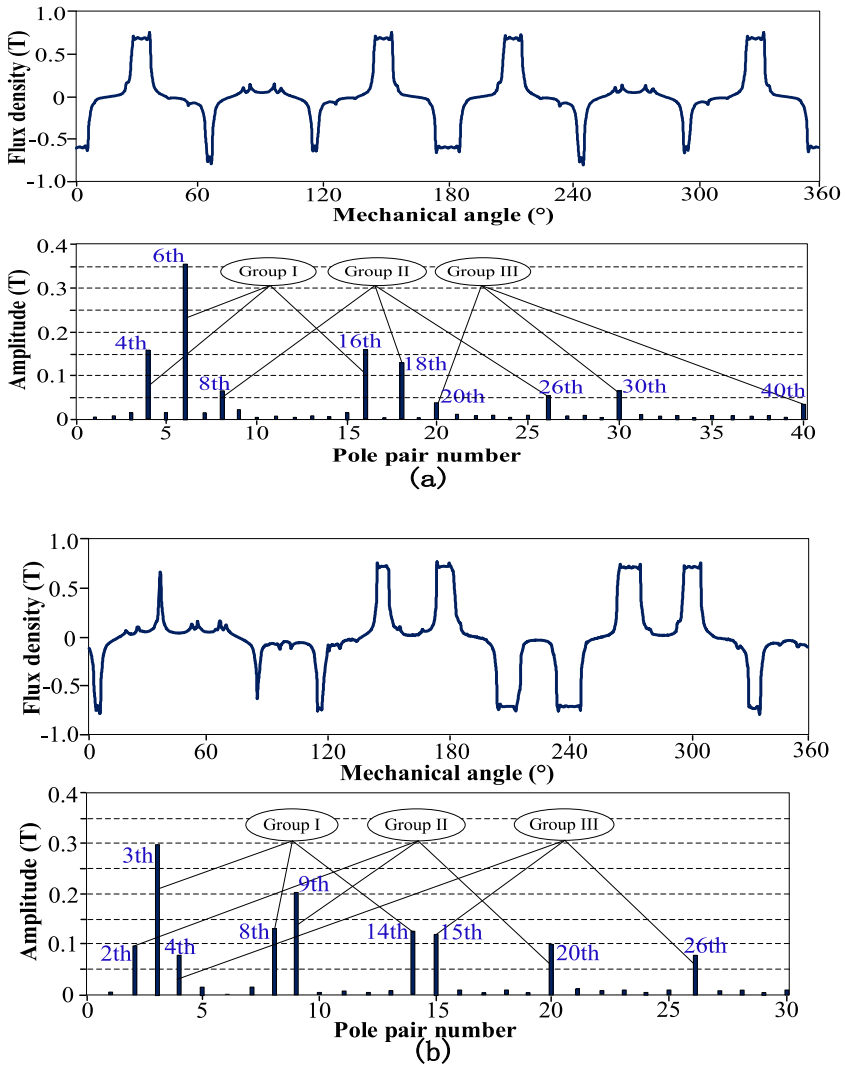

Fig. 5. Air gap flux density and FFT analysis of the magnetic field produced by two different DC layouts, after rotor modulation. (a) Existing. (b) Proposed.

9.43%.

4. Finite element verification

To verify the advantages of the proposed DC-VRM over the existing solution, their electromagnetic performance is further evaluated by using transient finite element analysis. The general design parameters for the two designs are presented in Table 3.

The no-load back EMF for two topologies both calculated as given in Fig. 6, at the speed of 900 rpm. The back EMF for the existing topology is around 54 V when a 6 A DC field current is applied. As for the proposed topology, two situations are considered for comparison. Firstly, when it is applied with the same DC field current 6 A, the back EMF of the proposed machine can achieve about 50 V, which means, although the DC coils are halved, the proposed design can still obtain a comparable excitation ability. Further, when the proposed topology is applied with 8.4 A DC field current, which generates the same DC copper loss as the existing topology, its back EMF achieves about 63 V. Therefore, the proposed topology can produce higher back EMF per DC copper loss, compared with the existing solution.

Further, the steady torque curves are calculated and presented in

Table 1
Harmonics contribution on EMF in the existing topology.

		PPN	B_{mn}	k_{wn}	EMF (%)
Group I	p_s	6	0.36	0.707	60.1
	$\|p_s - p_r\|$	4	0.16	0.866	17.2
	$p_s + p_r$	16	0.17	−0.5	6.7
Group II	$3p_s$	18	0.13	−0.707	7.9
	$\|3p_s - p_r\|$	8	0.07	0.5	1.1
	$3p_s + p_r$	26	0.07	−0.965	4.2
Group III	$5p_s$	30	0.06	−0.707	1.6
	$\|5p_s - p_r\|$	20	0.03	−0.866	0.6
	$5p_s + p_r$	40	0.03	0.5	0.2

Table 2
Harmonics contribution on EMF in the proposed topology.

		PPN	B_{mn}	k_{wn}	EMF (%)
Group I	p_s	3	0.29	0.923	65.7
	$\|p_s - p_r\|$	8	0.13	0.5	3.8
	$p_s + p_r$	14	0.13	−0.258	1.1
Group II	$3p_s$	9	0.21	0.383	6.1
	$\|3p_s - p_r\|$	2	0.09	0.966	6.9
	$3p_s + p_r$	20	0.10	−0.866	6.9
Group III	$5p_s$	15	0.12	−0.383	1.9
	$\|5p_s - p_r\|$	4	0.07	0.866	3.4
	$5p_s + p_r$	26	0.07	−0.966	4.1

Table 3
Some general dimension parameters for two DC-VRMs.

Parameter	Unit	Existing	Proposed
Outer diameter of stator	mm	150	
Outer diameter of rotor	mm	99	
Air gap length	mm	0.5	
Stack length	mm	80	
Number of stator teeth	–	12	
Arc of stator teeth	°	12	
Number of rotor poles		10	11
Arc of rotor pole	°	17	15
Slot factor	–	0.65	
Current density		6	
Wire size (AWG)	–	20	
Turns of one phase winding		200	
Turns of DC field winding	–	600	300

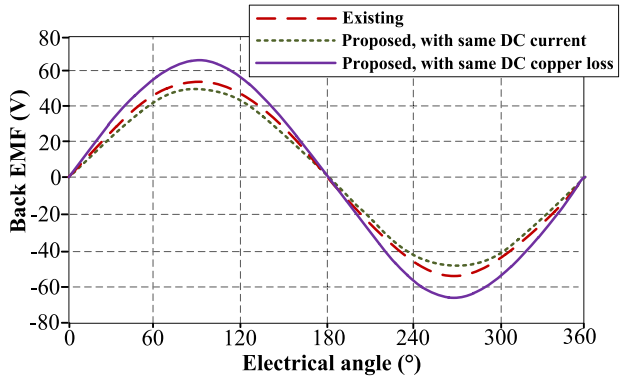

Fig. 6. Back EMF waveforms, at the speed 900 rpm.

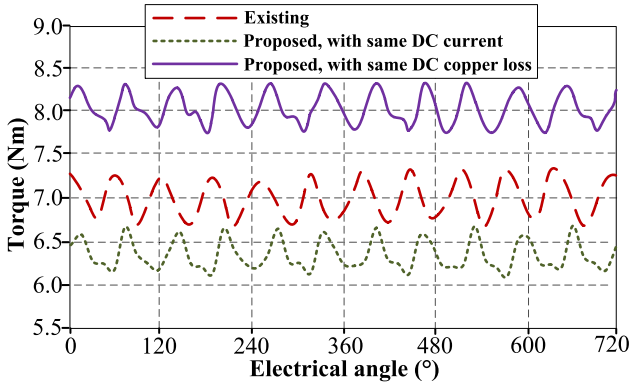

Fig. 7. Steady torque waveforms.

Fig. 7. with 8.4 A sinusoidal armature current injected. It can be noticed that about 14.8% higher output torque can be achieved in the proposed topology when DC copper loss maintains the same.

Finally, the total copper loss, core loss and output mechanical power are all evaluated and presented in Fig. 8. Based on these data, the machine efficiency can also be calculated as 79.7% for the existing topology, 82.4% for the proposed topology with the same DC current, and 82.1% for the proposed topology with the same DC copper loss. Therefore, the proposed DC-VRM with halved DC coils can provide higher efficiency than the existing solution and thus is a more efficient non-PM candidate.

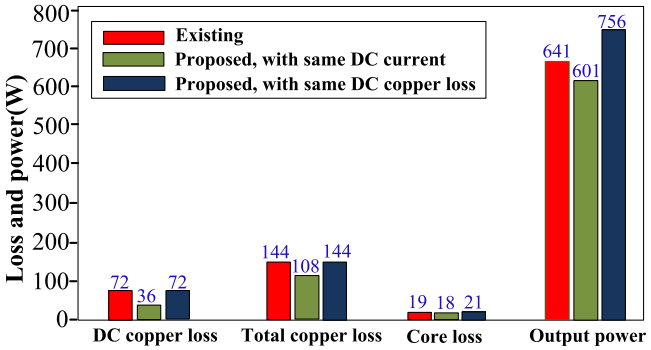

Fig. 8. Loss and power evaluation.

5. Conclusion

This paper proposes an efficiency-enhanced DC-VRM. The key is based on the flux modulation mechanism to reduce DC field coils and mitigate DC copper loss. In this paper, the influence of two different DC layouts is quantitatively analyzed based on a magneto-static finite element and analytical combined method, which reveals that, with DC field coils halved in the proposed solution, the contribution of fundamental DC field harmonic is reduced, while that of third-order and fifth-order harmonics are both increased. Therefore, a comparable excitation ability and torque density can still be achieved in the proposed design with DC coils halved. Further, a transient finite element comparison is performed, and it proves that the proposed design can achieve higher back EMF and output torque per DC copper loss. Hence, this new efficiency-enhanced DC-VRM topology can be a more promising non-PM candidate for EV propulsion.

Declaration of competing interest

The authors declare no conflict of interest.

Data availability

Data will be made available on request.

Acknowledgments

This work was supported by the Research Project Polyu 152109/20E, Hong Kong Polytechnic University, Hong Kong, and RGC Collaborative Research Fund (CRF) C1052-21G.

References

[1] Boldea, I., Tutelea, L.N., Parsa, L., 2014. Automotive electric propulsion systems with reduced or no permanent magnets: an overview. IEEE Trans Ind Electron 61 (10), 5696–5711.
[2] Tang, Y., Kline, J.A., 1996. Modeling and design optimization of switched reluctance machine by boundary element analysis and simulation. IEEE Trans Energy Convers 11 (4), 673–680.
[3] Liu, Yaguang, Pillay, P., 2004. Improved torque performance of switched reluctance Machines by reducing the mutual saturation effect. IEEE Trans Energy Convers 19 (2), 251–257.
[4] Rahman, K.M., Schulz, S.E., 2002. Design of high-efficiency and high-torque-density switched reluctance motor for vehicle propulsion. IEEE Trans Ind Appl 38 (6), 1500–1507.
[5] Kiyota, K., Kakishima, T., Chiba, A., 2014. Comparison of test result and design stage prediction of switched reluctance motor competitive with 60-kW rare-earth PM motor. IEEE Trans Ind Electron 61 (10), 5712–5721.
[6] Yu, L., Zhang, Z., Chen, Z., Yan, Y., 2014. Analysis and verification of the doubly salient brushless DC generator for automobile auxiliary power unit application. IEEE Trans Ind Electron 61 (12), 6655–6663.
[7] Lee, C.H.T., Chau, K.T., Liu, C., Ching, T.W., Li, F., 2014. Mechanical offset for torque ripple reduction for magnetless double-stator doubly salient machine. IEEE Trans Magn 50 (11), 1–4.

[8] Liu, X., Zhu, Z.Q., 2013. Comparative study of novel variable flux reluctance machines with doubly fed doubly salient machines. IEEE Trans Magn 49 (7), 3838–3841.
[9] Huang, L.R., Feng, J.H., Guo, S.Y., Shi, J.X., Chu, W.Q., Zhu, Z.Q., 2017. Analysis of torque production in variable flux reluctance machines. IEEE Trans Energy Convers 32 (4), 1297–1308.
[10] Jia, S., Qu, R., Li, J., Li, D., Lu, H., 2017. Design considerations of stator DC-winding excited vernier reluctance machines based on the magnetic gear effect. IEEE Trans Ind Appl 53 (2), 1028–1037.
[11] Zhao, X., Wang, S., Niu, S., Fu, W., Zhang, X., 2022. A novel high-order-harmonic winding design method for vernier reluctance machine with dc coils across two stator teeth. IEEE Trans Ind Electron 69 (8), 7696–7707.
[12] S. Jia, R. Qu, J. Li, Y. Chen, Comparison of stator dc-excited vernier reluctance machines with synchronous reluctance machines, in: 2015 IEEE international electric machines & drives conference (IEMDC), Coeur d'Alene, ID, USA, 2015, pp. 649–655.
[13] Jia, S., Qu, R., Li, J., 2015. Analysis of the power factor of stator DC-excited vernier reluctance machines. IEEE Trans Magn 51 (11), 8207704, pp. 1–4.
[14] Zhao, X., Niu, S., 2017. Design and optimization of a new magnetic-geared pole-changing hybrid excitation machine. IEEE Trans Ind Electron 64 (12), 9943–9952.
[15] Huang, J., Fu, W., Niu, S., Zhao, X., 2021. Comparative analysis of different permanent magnet arrangements in a novel flux modulated electric machine. IEEE Access 9, 14437–14445.
[16] Niu, S., Sheng, T., Zhao, X., Zhang, X., 2019. Operation principle and torque component quantification of short-pitched flux-bidirectional-modulation machine. IEEE Access 7, 136676–136685.